

Experimental study on flexural behavior of splicing concrete-filled GFRP tubular composite members connected with steel bars

B.L. Chen* and L.G. Wang

College of Resources and Civil Engineering, Northeastern University, Shenyang 110819, P.R. China

(Received May 23, 2013, Revised October 05, 2014, Accepted November 18, 2014)

Abstract. Based on the experiment, this paper focuses on studying flexural behavior of splicing concrete-filled glass fiber reinforced polymer (GFRP) tubular composite members connected with steel bars. The test results indicated the confinement effects of GFRP tubes on the concrete core in compression zone began to produce, when the load reached about 50% P_u (P_u -ultimate load), but the confinement effects in tensile zone was unobvious. In addition, the failure modes of composite members were influenced by the steel ratio of the joint. For splicing unreinforced composite members, the steel ratio more than 1.96% could satisfy the splicing requirements and the steel ratio 2.94% was ideal comparatively. For splicing reinforced specimen, the bearing capacity of specimen with 3.92% steel ratio was higher 21.4% than specimen with 2.94% steel ratio and the latter was higher 21.2% than the contrast non-splicing specimen, which indicated that the steel ratio more than 2.94% could satisfy the splicing requirements and both splicing ways used in the experiment were feasible. So, the optimal steel ratio 2.94% was suggested economically. The experimental results also indicated that the carrying capacity and ductility of splicing concrete-filled GFRP tubular composite members could be improved by setting internal longitudinal rebars.

Keywords: connect with steel bars; concrete-filled GFRP tube; experimental study; flexural behavior; splicing

1. Introduction

Concrete-filled glass fiber reinforced polymer (GFRP) tubular (CFGF) composite member is a new kind of composite member, which is formed by pouring concrete into GFRP tube (Qin 2009, Chen *et al.* 2010). This kind of composite member makes full use of GFRP tube to confine concrete core, so that concrete core is under a three-dimensional stress state, while GFRP tube is under hoop tension in the lateral direction (Xiao and Wu 2003, Fujikake *et al.* 2004, Shao and Mirmiran 2005, Cho *et al.* 2005, Matthys *et al.* 2005, Saenz and Pantelides 2007, Mehrdad and Mohammad 2009, Wang *et al.* 2011). Besides, the ductility of concrete core is improved and the stability of thin-walled GFRP tube is also enhanced (Saadatmanesh and Ehsani 1994, Mirmiran *et al.* 1999). And especially, GFRP tube with superior corrosion resistance can provide lightweight

*Corresponding author, Associate Professor, E-mail: chenbailing@mail.neu.edu.cn

formwork during construction and life-long protection for concrete core in harsh environments (Lu 2005, Salim *et al.* 2006, Wang and Wang 2009). For CFGT, the ideal force state is under axial compression while in practical applications, CFGT is generally under eccentric compression, compressed bending, even pure bending, which is due to design, construction and material defects etc. (Moran and Pantelides 2002, Lam and Teng 2004, Liu and Lu 2010, Hu *et al.* 2011, Xiong *et al.* 2012, Bousselham and Chaallal 2006, Hoult and Lees 2009, Manjunatha *et al.* 2010, Panda *et al.* 2012). In recent years, the flexural behaviors of CFGT composite members have been studied by many experts and scholars all over the world (Davol *et al.* 2001, Fam and Rizkalla 2002, Cole and Fam 2006, Yu *et al.* 2006). Mainly, based on the bending test of CFGT member, the influences of winding angle of the fiber tube, steel ratio, loading method, shear-span ratio on flexural behavior and working mechanism of composite members have been studied, and the corresponding calculation formulas of flexural bearing capacity have also been given. But the study on splicing CFGT composite member is seldom. Helmi *et al.* (2005) made experiments on splicing CFGT specimen 13,700 mm length. Based on 3-divided-point test, the experimental results showed the bearing capacity of splicing CFGT specimen was about 7% higher than that of non-splicing specimen. The failure appeared at the joint, which was primarily attributed to the fracture of the connecting reinforcement. Zhu *et al.* (2006) did some research on splicing techniques for precast concrete-filled fiber-reinforced polymer (FRP) tubes (CFFT). A total of four spliced beams were tested. Three were internally spliced using grouted steel bars, grouted FRP bars, or unbonded post-tensioning bars, and the fourth was spliced with FRP socket. A control CFFT beam with no internal reinforcement was also tested as a reference. The loading mode of all specimens was 4-divided-point loading. The experimental results showed that all specimens had good continuity and the connection mode was feasible.

Despite significant advances in the research of CFGT composite members, still for the structure system to be used in either bridge or building construction, appropriate connections, which are considered as critical components of the entire structure system, need to be developed. Furthermore, these joints are just the key positions of CFGT composite members and their load-carrying capabilities are more complicated than other parts of the continuous members. Therefore, it is very necessary to study the mechanical performances of splicing CFGT composite members. Based on the experiment and taking the connecting reinforcement ratio as the main parameter, this paper focuses on studying the flexural behaviors of splicing CFGT composite members connected with steel bars.

2. Experimental program

2.1 Materials and parameters

A total of seven specimens were tested in the experimental program, including three splicing unreinforced CFGT specimens (BCS(T)-1, BCS(T)-2 and BCS(T)-3) spliced using steel bars at their mid-length, in comparison with one non-splicing specimen (BCS(T)-6) with no internal reinforcement; and two splicing reinforced CFGT specimens (BRCS(T)-1 and BRCS(T)-2) connected using steel bars at their mid-length, in comparison with one non-splicing reinforced specimen (BRCS(T)-5). The inner diameter and wall thickness of all GFRP tubes used in the experimental program were 200 mm and 5.5 mm respectively. The fiber winding angle of all GFRP tubes was 80°, and the measured compressive strength of concrete of all specimens was

40.8 MPa. The diameters of all longitudinal steel bars (including middle connecting rebars) and stirrups were respectively 14 mm and 8 mm. The total length of all specimens, among which all splicing specimens were formed from two GFRP tubes 700 mm length connected together at their ends by rebar connector, is 1,400 mm. The material properties are shown in Table 1, and the other experimental parameters used in the experimental program are given in Table 2. Besides, Fig. 1 shows the forms of GFRP tubes and connectors.

2.2 Fabrication of specimens

GFRP tubes and connectors used in this experimental program can be seen in Fig. 1. Before casting, axial and lateral strain gauges were mounted along the hoop directions on the external surface of the specimens at the mid-length and quarter length. Also axial and lateral strain gauges were installed on the hoop and longitudinal steel bars of the connectors, as shown Figs. 1(b)-(g). Next, concrete was poured into one GFRP tube (700 mm length) and vibrated densely. Then, one end of the banded steel reinforcement cage (connector) was inserted into concrete and made sure the cage put into half length of GFRP tube and placed in the middle. After that, filled the

Table 1 Material properties

Specimen	Measured compressive strength of concrete (MPa)	GFRP tube			Diameter of steel bar (mm)	Diameter of stirrup (mm)
		Inner diameter (mm)	Wall thickness (mm)	Winding angle of fiber (°)		
BCS(T)-1	40.8	200	5.5	80	14	8
BCS(T)-2	40.8	200	5.5	80	14	8
BCS(T)-3	40.8	200	5.5	80	14	8
BCS(T)-6	40.8	200	5.5	80	14	8
BRCS(T)-1	40.8	200	5.5	80	14	8
BRCS(T)-2	40.8	200	5.5	80	14	8
BRCS(T)-5	40.8	200	5.5	80	14	8

Table 2 Chart of experimental parameters

Specimen	Number of continuous longitudinal rebar	Length of continuous longitudinal rebar (mm)	Number of middle connecting rebar	Length of middle connecting rebar (mm)	Steel ratio (%)	Specimen type	Bearing capacity (kN)
BCS(T)-1	—	—	4	700	1.96	splicing	69
BCS(T)-2	—	—	6	700	2.94	splicing	98
BCS(T)-3	—	—	8	700	3.92	splicing	64
BCS(T)-6	—	—	—	—	—	non-splicing	41
BRCS(T)-1	4	1400	2	700	2.94	splicing	103
BRCS(T)-2	4	1400	4	700	3.92	splicing	125
BRCS(T)-5	4	1400	—	—	1.96	non-splicing	85

GFRP tube with concrete and vibrated concrete fully, and put another GFRP tube (700 mm length) on the foregoing filled one. Finally, pouring concrete into the latter GFRP tube until GFRP tube was filled with concrete completely and vibrated densely. After flattening the surface of poured concrete, the splicing CFGT composite member connected with steel bars was fabricated. Fig. 1(h) shows fabricated specimens in the test.

2.3 Test contents and methods

The main contents of this experiment include:

- (1) Obtain the loads applied on specimens;
- (2) Measure the strains of longitudinal reinforcements and stirrups;
- (3) Measure the hoop and longitudinal strains of GFRP tubes;
- (4) Observe the lateral deflection of specimens.



(a) GFRP tubes



(b) Connector for BCS(T)-1 (700 mm length)



(c) Connector for BCS(T)-2 (700 mm length)



(d) Connector for BCS(T)-3 (700 mm length)

Fig. 1 Forms of GFRP tubes and connectors



(e) Connector for BRCS(T)-1 (1,400 mm length)



(f) Connector for BRCS(T)-2 (1,400 mm length)



(g) Connector for BRCS(T)-5 (1,400 mm length)



(h) Fabricated specimens

Fig. 1 Continued

Layout of strain gauges can be seen in Figs. 1(b)-(g) and Fig. 2. And Fig. 2 also shows the arrangement schematic of displacement meters which are respectively 200 mm, 400 mm from both ends of specimen and at mid-span.

All specimens were loaded at mid-span and the concentrated load acted vertically downwards perpendicular to the axis of specimens, using testing machine with a 5,000-kN capacity by monotonous grading loading. During loading, a piece of steel base-plate, under which two semicircle steel hoops with 100 mm inner radius was welded, was put under the loading point in order to fix specimen and transmit the load. The procedure was:

- (1) Specimen was placed on both supports of test-bed and geometrically in the middle;
- (2) Preloading and checking if the test instrument worked properly, then unloading to zero;

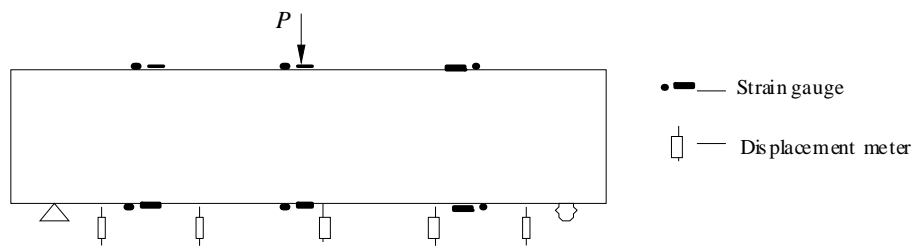


Fig. 2 Layout of displacement meter and strain gauges



Fig. 3 Photograph of test setup and loading

- (3) Monotonous grading loading: load was applied at an increment of 4-kN at the early stage of loading; when the loads reached about 70% of the expected ultimate load of the specimen, the loading speed slowed down and the loading increment was changed to 2-kN; close to the failure, load continuously and slowly until the specimen damaged. All the strain readings were recorded by a data acquisition system connected to a computer during loading. Fig. 3 shows the test setup and loading.

3. Experimental phenomena and discussion

At the early stages of loading, the overall behavior was similar for all specimens. The deformation of GFRP tube, internal reinforcement and concrete was very small and the specimens were in the elastic stage. The joint is under coordination work just like the continuous body.

For specimen BCS(T)-1 (steel ratio 1.96%): as the load approached about 50% P_u , the cracks began to appear at the joint of specimen. With the increase of load, the cracks gradually grew. When the load reached 65% P_u , the slip began to appear between GFRP tube and concrete at the joint. And the fiber began to send out frequent noise with the increase of load. Until the load reached the ultimate load 69 kN, GFRP tube and concrete in compression zone were crushed and the tensile reinforcement was stretched to break. Fig. 4(a) shows the failure mode of specimen BCS(T)-1.

For specimen BCS(T)-2 (steel ratio 2.94%): as the load approached about 60% P_u , the cracks began to appear at the joint of specimen. With the increase of load, the cracks gradually grew. When the load reached 82% P_u , some white stripes appeared on the surface of GFRP tube in tensile zone near the end of connecting steel bars (about 390 mm from one end of specimen). And with the continuous increase of load, the white stripes became obvious with frequent noise while the

cracks of concrete in the joint developed hardly. Approaching the ultimate load, the fiber of GFRP tube (390 mm from one end of specimen) in tensile zone began to crack, and GFRP tube and concrete in compression zone were crushed simultaneously. When the load reached the ultimate load 98 kN, the specimen failed and the tensile reinforcement in the connection yielded but was not stretched to break. Fig. 4(b) shows the failure mode of specimen BCS(T)-2.

For specimen BCS(T)-3 (steel ratio 3.92%): as the load approached about 60% P_u , some white stripes appeared on the surface of GFRP tube in tensile zone near the end of connecting steel bars (about 350 mm from one end of specimen). When the load is up to 72% P_u , the concrete began to crack. With the increase of load, the cracks of the concrete enlarged. Until the ultimate load 64 kN, GFRP tube and concrete in compression zone were crushed. During the whole bearing-force process, there was no any damaged phenomenon in the joint part. Fig. 4(c) shows the failure mode of specimen BCS(T)-3.

For specimen BCS(T)-6 (comparison specimen): as the load approached about 50% P_u , some white stripes began to appear on the surface of GFRP tube in tensile zone at mid-span of specimen. With the increase of load up to about 80% P_u , GFRP tube and concrete cracked. When the load reached the ultimate load 41 kN, GFRP tube and concrete in compression zone were crushed, and the specimen failed. Fig. 4(d) shows the failure mode of specimen BCS(T)-6.

For specimen BRCS(T)-1 (steel ratio 2.94%): as the load approached about 30% P_u , the cracks began to appear in the joint. With the increase of load, the width of the cracks enlarged. But no slippage appeared between GFRP tube and concrete. When the load reached the ultimate load 103 kN, inner tensile reinforcement got stretched to break. Fig. 4(e) shows the failure mode of specimen BRCS(T)-1.

For specimen BRCS(T)-2 (steel ratio 3.92%): as the load approached about 30% P_u , there were tiny cracks appearing in the joint and there was minor slippage between GFRP tube and concrete. When the load reached about 70% P_u , the fiber and resin of GFRP tube began to send out frequent cracking noise, and at the same time some white stripes appeared on the top surface of GFRP tube in the joint. Until the load increased to the ultimate load 125 kN, concrete of the joint in tensile zone got cracked and that in compression area got crushed. Fig. 4(f) shows the failure mode of specimen BRCS(T)-2.

For specimen BRCS(T)-5 (steel ratio 1.96%, comparison specimen): as the load approached about 40% P_u , some white stripes appeared on the surface of GFRP tube of mid-span in tensile zone, and also the fiber and resin of GFRP tube began to send out frequent cracking noise. In addition, with the increase of load, white stripes became more obvious. Until the load increased to the ultimate load 85 kN, GFRP tube being 50 mm from mid-span in tensile zone was stretched to break, and simultaneously GFRP tube and concrete in compression zone were crushed. Fig. 4(g) shows the failure mode of specimen BRCS(T)-5.

Based on the failure modes of unreinforced CFGT members above, specimen BCS(T)-1 failed in the joint, while specimen BCS(T)-2 and BCS(T)-3 did not fail in the joint. But the ultimate load of all the three splicing specimens was higher than the comparison specimen (BCS(T)-6), and at least higher about 56%. The test result showed the failure mode and bearing capacity were influenced by the steel ratio of the connecting rebars in the joint, and the steel ratio used in the experiment could ensure normal work of CFGT composite member. The steel ratio 2.94% was ideal and suggested.

For reinforced CFGT members, all of three specimens failed in the joint. The bearing capacity of specimen BRCS(T)-2 (125 kN) was higher 21.4% than specimen BRCS(T)-1 (103 kN), and the latter was higher 21.2% than the contrast specimen BRCS(T)-5 (85 kN). The result indicated that

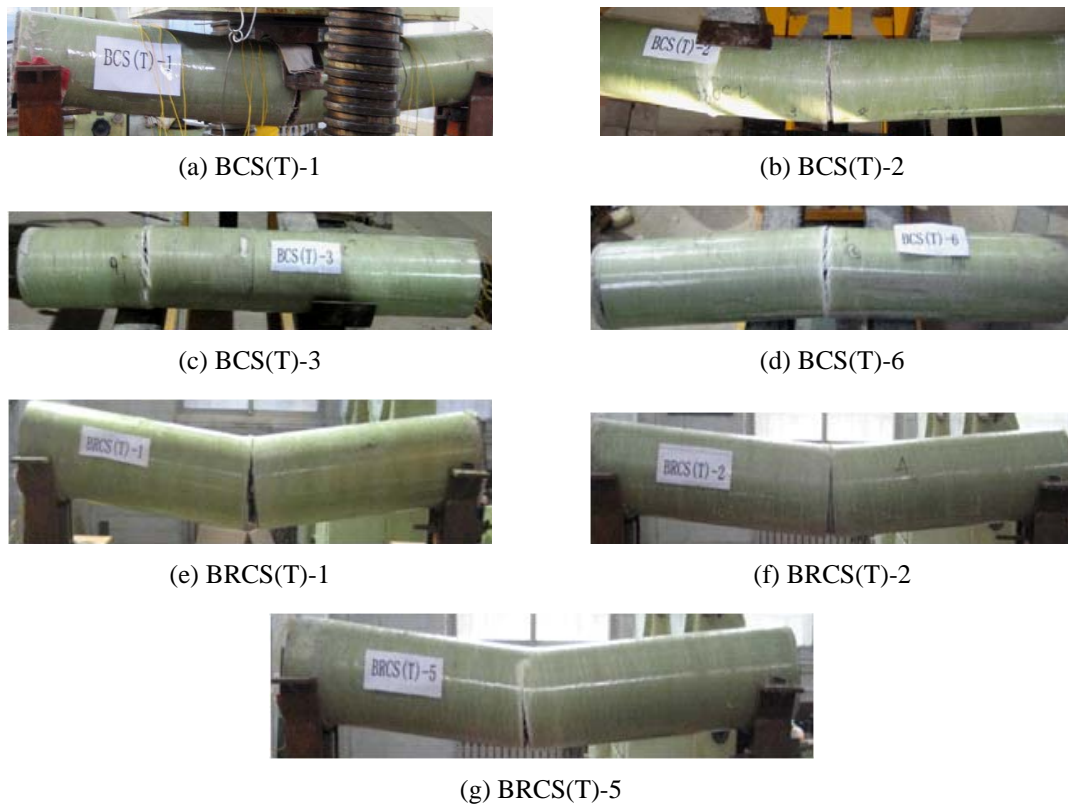


Fig. 4 Failure modes of specimens

the steel ratio more than 2.94% could satisfy the splicing requirements and both splicing ways used in the experiment could ensure normal work of splicing composite members. So, economically the optimal steel ratio 2.94% was suggested.

4. Load-deformation behavior

Fig. 5 shows the relationship curves of mid-span deformation (u) and load (F) for all specimens in this experiment. The result indicates that the relation curves are composed of three stages (straight line segment, curve segment of the elastic-plastic stage and oblique straight line segment of limit state) during the whole loading. At the early stages of loading, the deformation of all specimens showed a similar linear growth tendency. It showed that GFRP tube, concrete and reinforcements of joint could coordinate with each other like other continuous parts during this phase. When the load reached $0.45\text{--}0.55P_u$ (BCS(T)-1 at $0.55P_u$, BCS(T)-2 at $0.47P_u$, BCS(T)-3 at $0.47P_u$, BRCS(T)-1 at $0.54P_u$, BRCS(T)-2 at $0.51P_u$), the increasing speed of the deformation was obviously greater than that of the load, and the load-deformation curve presented a nonlinear growth tendency. With the continuous increase of the load, the load-deformation curve presented a linear growth tendency and the bearing capacities of specimens increased slowly while the deformations increased rapidly. In addition, for unreinforced CFGT specimens, the deformation of

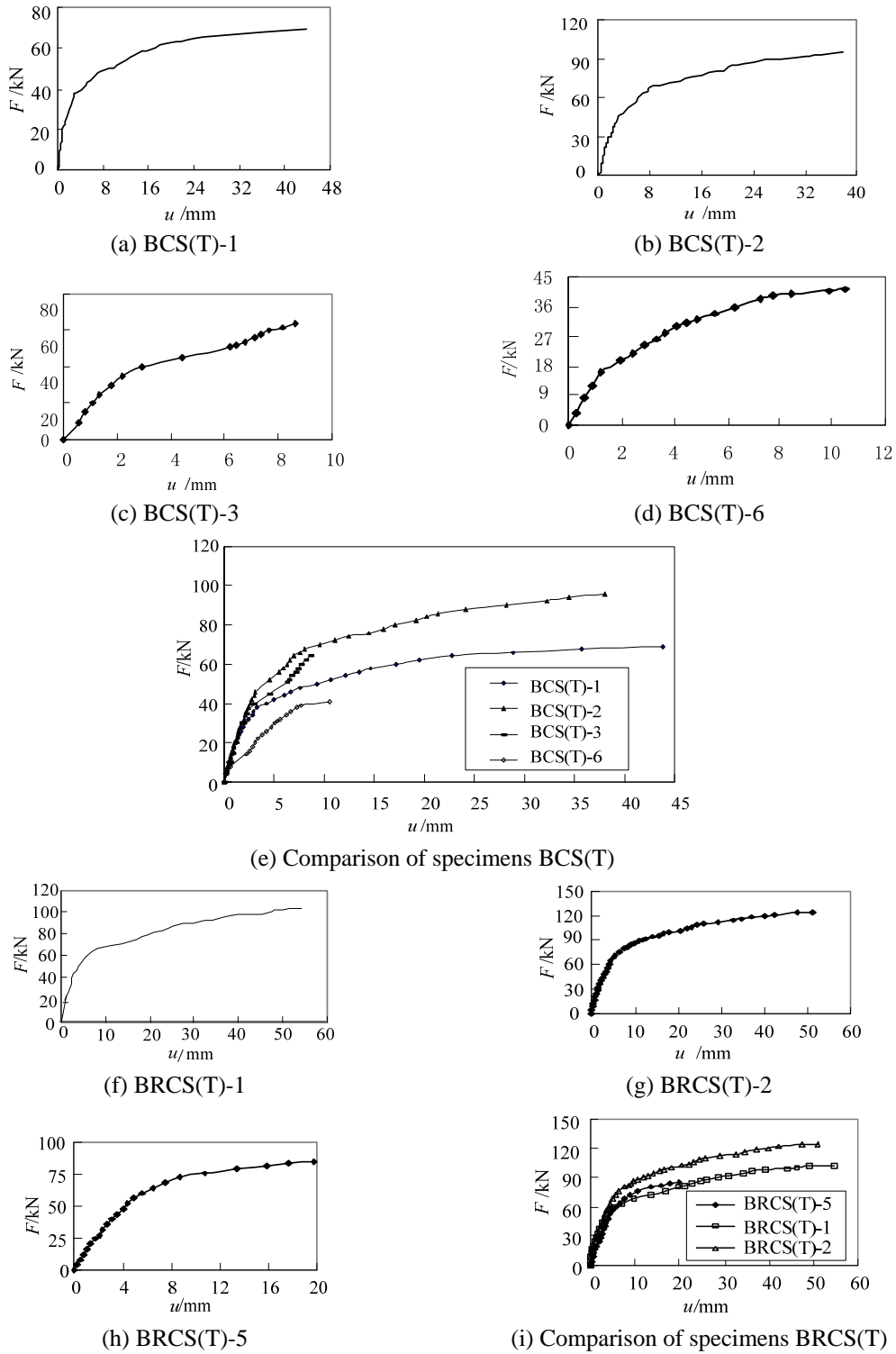


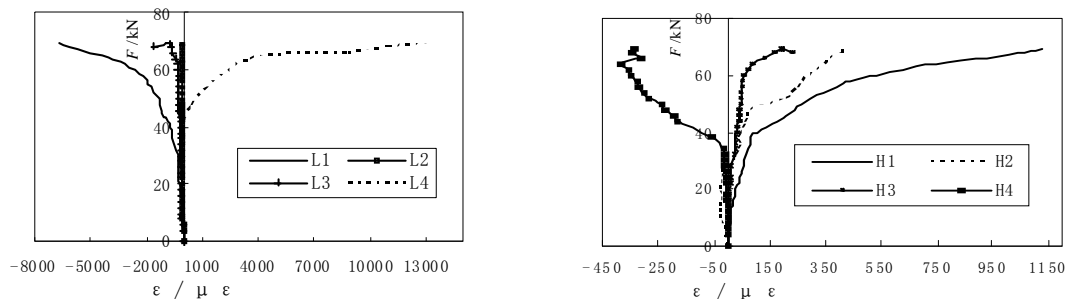
Fig. 5 Relationship curves of load-deflection at mid-span

specimens BCS(T)-1 and BCS(T)-2 was larger than specimens BCS(T)-3 and BCS(T)-6 at the ultimate state. It showed that the ductility of specimens BCS(T)-1 and BCS(T)-2 was better than specimens BCS(T)-3 and BCS(T)-6, and the bearing capacity of specimen with steel ratio 2.94% was more reasonable than steel ratio 1.96% and 3.92%. For reinforced CFGT specimens, the deformation of splicing specimens BRCS(T)-1 and BRCS(T)-2 was larger than non-splicing specimen BRCS(T)-5 at the ultimate state. It showed that the ductility of splicing specimens BRCS(T)-1 and BRCS(T)-2 was better than non-splicing specimen BRCS(T)-5. The experimental results also show the bearing capacity and ductility of reinforced CFGT composite members are better than unreinforced ones. Based on the same steel ratio, the bearing capacity of reinforced CFGT composite members is at least higher 5% than unreinforced ones.

5. Load-strain behavior

The longitudinal and hoop strains of GFRP tube of quarter length and joint (mid-span) were mainly tested in this experiment. Fig. 6 shows the curves of the longitudinal and hoop strains. Strain values in tensile zone and compressive zone were assumed positive and negative, respectively. The results showed the strains of GFRP tube at the quarter length developed more obviously, and the major performances as follows:

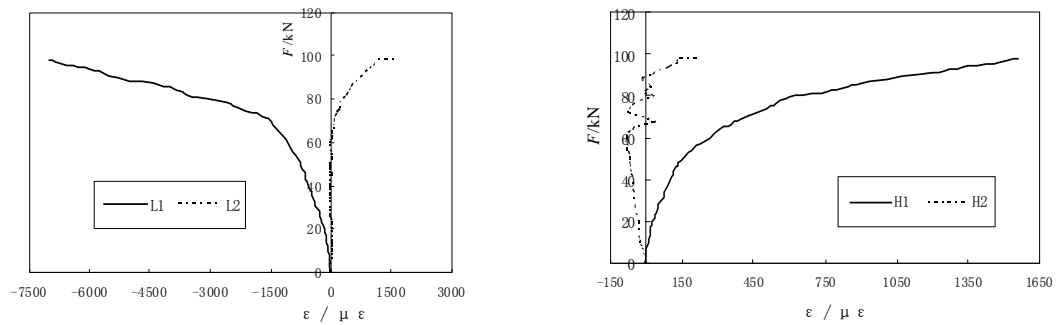
- (1) The longitudinal strain of GFRP tube: The longitudinal strain of GFRP tube in compressive zone, at the early stage of loading, was very small. Until the load was up to about $80\%P_u$, the increase of the strain became obvious and the largest compressive strain tested was about 7,500; the longitudinal strain of GFRP tube in tensile zone, at the early stage of loading, was also very small. Until the load was up to about $90\%P_u$, the increasing speed of the strain became fast and was higher than that of load. The relationship between the load and the strain was near liner. That was due to the poor tensile capacity of concrete, and after concrete in tension zone quit working, the tensile force was mainly carried by GFRP tube. The maximum tensile strain tested reached about 13,000.
- (2) The hoop strain of GFRP tube: The hoop strain of GFRP tube in compressive zone, at the early stage of loading, increased linearly with the growth of load. And GFRP tube in compressive zone was stretched along hoop direction. As the load increased about $50\%P_u$,



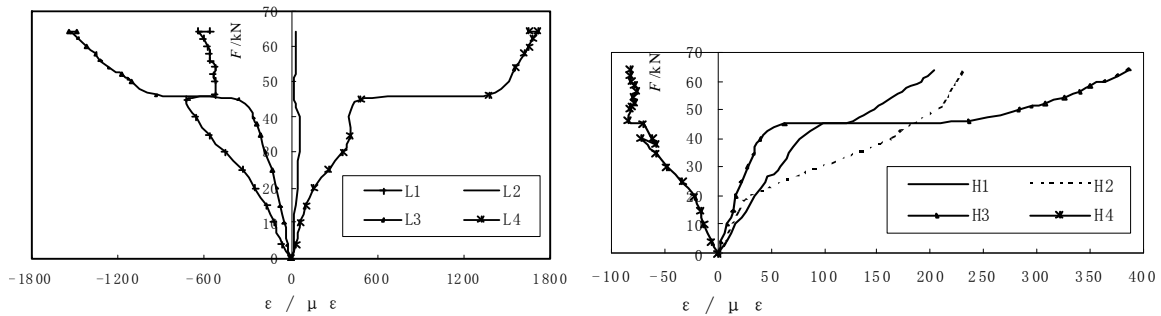
(a) BCS(T)-1

Fig. 6 Load-strain curves

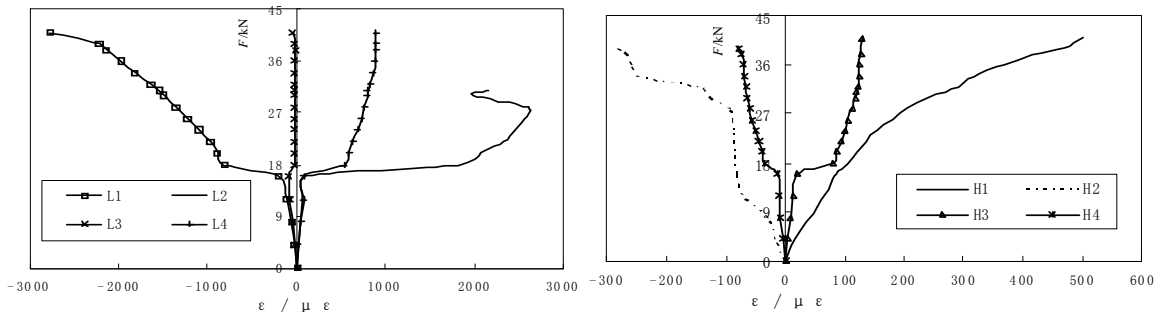
the confinement effect of GFRP tube on concrete began to produce, which led to the inner concrete being in three-dimensional state of compression. With the increase of load, the volume of concrete expanded rapidly and the hoop strain of GFRP tube increased continuously so that the confinement effect got further strengthened. The experimental result also showed GFRP tube in tensile zone was compressed along hoop direction, which was due to GFRP tube in this zone was stretched in longitudinal direction. There was no confinement effect of GFRP tube on concrete in tensile zone, and GFRP tube and concrete carried load independently. In other words, there was no interaction between GFRP tube



(b) BCS(T)-2



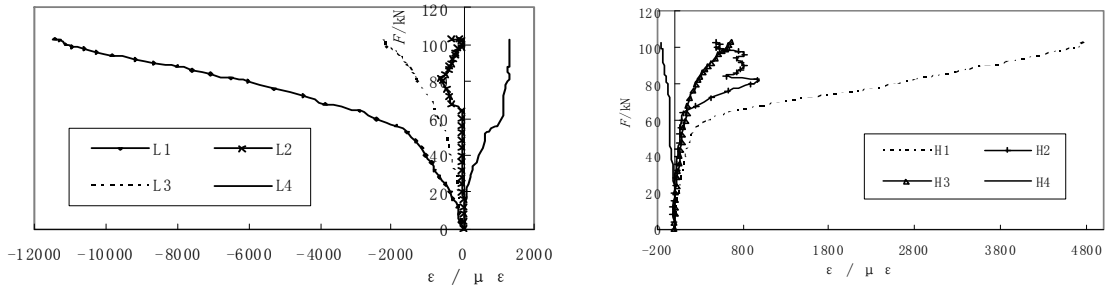
(c) BCS(T)-3



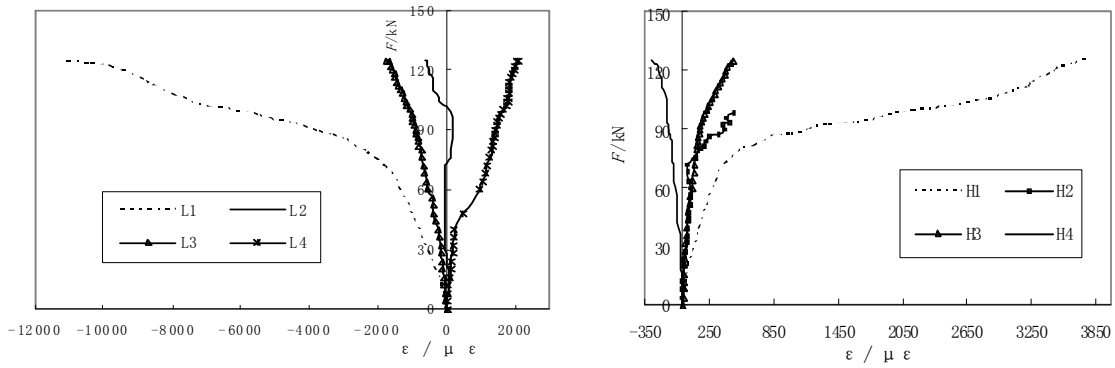
(d) BCS(T)-6

Fig. 6 Continued

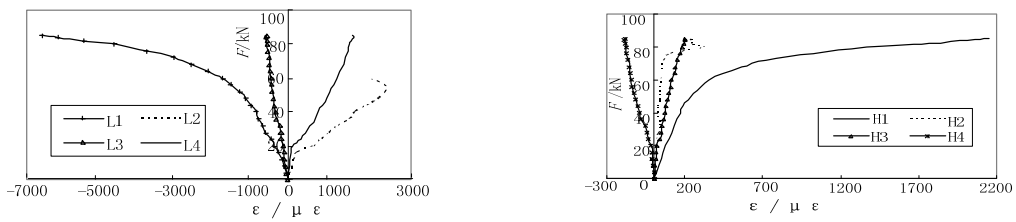
and concrete in tensile zone. The maximum hoop strain tested was about 1,200. GFRP tube at the mid-span (the joint) was unconfined, which led to the longitudinal and hoop strain of GFRP tube here exhibiting irregularly and the strain values being very small.



(e) BRCS(T)-1



(f) BRCS(T)-2



(g) BRCS(T)-5

Fig. 6 Continued

Footnotes: L1 = longitudinal strain of mid-span in compressive zone;
 L2 = longitudinal strain of mid-span in tensile zone;
 L3 = longitudinal strain of quarter length in compressive zone;
 L4 = longitudinal strain of quarter length in tensile zone;
 H1 = hoop strain of mid-span in compressive zone;
 H2 = hoop strain of mid-span in tensile zone;
 H3 = hoop strain of quarter length in compressive zone;
 H4 = hoop strain of quarter length in tensile zone.

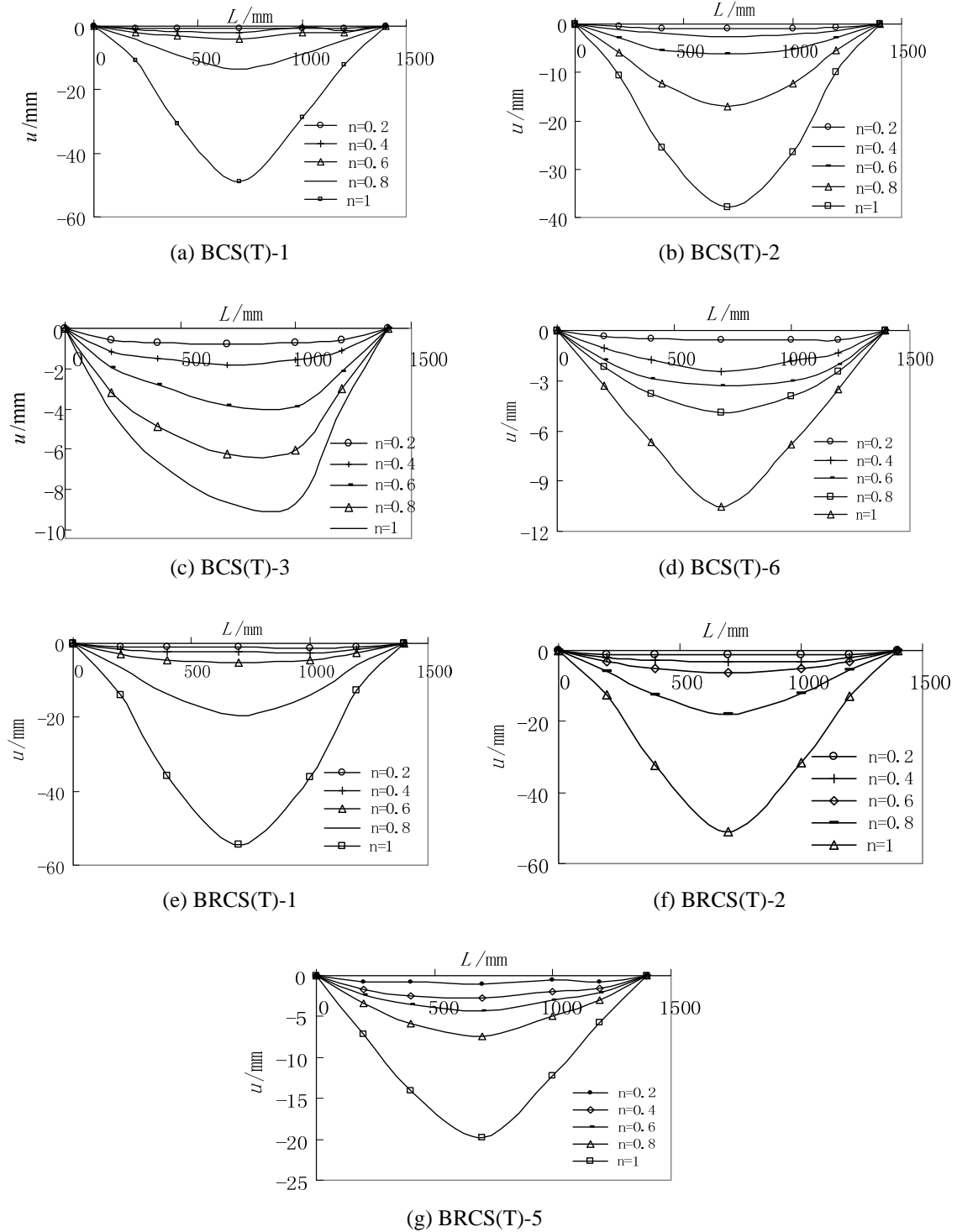


Fig. 7 Lateral deflection curves of specimens

6. Lateral deflection

Fig. 7 shows the lateral deflection curves of specimens. The value of n is the ratio of the load (F_0) and the ultimate load (F_u) during each stage. The abscissa is the location of displacement meter (L) along the length direction of specimens and the abscissa values (0 and 1,400 mm) correspond to both ends of each specimen. The ordinate is the deflection value u in different location of displacement meter during the process of loading.

Fig. 7 exhibits the lateral deflection curves of all specimens correspond to similar law. At the early stage of loading, the amplitude of variation of lateral deflection was smaller, and the lateral deflection of specimen at bilateral symmetrical position of mid-span was basically same. With the increase of load, the value of lateral deflection went increasing, and the lateral deflection curve was approaching to bilateral symmetry and gradually to half-sinusoid.

7. Conclusions

Based on the research work above, the following conclusions have been drawn:

- (1) Splicing unreinforced CFGT composite members: The failure mode was influenced by the steel ratio of the connecting rebars in the joint. The steel ratio 2.94% was ideal. In addition, the carrying capacity of all the three splicing specimens was higher than the contrast specimen and at least higher 56%, which showed that the steel ratio used in this experiment program could satisfy the design requirements. The least steel ratio 1.96% suggested was advisable.
- (2) Splicing reinforced CFGT composite members: The carrying capacity of the specimen with the steel ratio 3.92% was higher 21.4% than the specimen with the steel ratio 2.94% and the latter was higher 21.2% than the contrast specimen, which showed that both splicing ways used in the experiment program was feasible and economically the optimal steel ratio 2.94% was suggested.
- (3) The bearing capacity and ductility of splicing specimens were better than non-splicing specimen, and the reinforced CFGT composite members are better than unreinforced ones. Based on the same steel ratio, the bearing capacity of reinforced CFGT composite members is at least higher 5% than unreinforced ones. The results indicated that the carrying capacity and ductility of CFGT composite member could be improved by setting internal longitudinal reinforcement.
- (4) The lateral deflection curves of all specimens correspond to similar law. At the early stage of loading, the amplitude of variation of lateral deflection was smaller, and the lateral deflection of specimen at bilateral symmetrical position of mid-span was basically same. With the increase of load, the value of lateral deflection went increasing, and the lateral deflection curve was approaching to bilateral symmetry and gradually to half-sinusoid.

Acknowledgments

The research described in this paper was financially supported by the China Scholarship Council (No. 201406085029), the Fundamental Research Funds for the Central Universities (N120401010), the Doctoral Fund of National Ministry of Education (No. 20050145012) and the Natural Science Foundation of Liaoning Province (No. 20052019).

References

- Bousselham, A. and Chaallal, O. (2006), "Behavior of reinforced concrete T-beams strengthened in shear with carbon fiber reinforced polymer-an experimental study", *ACI Struct. J.*, **103** (3), 339-347.
- Chen, B.L., Wang, L.G. and Qin, G.P. (2010), "Experimental research on anti-bending performance of composite RC-Filled GFRP tube members", *J. Northeast. Univ. (Natural Science)*, **31**(10), 1495-1498. [In Chinese]
- Cho, C.G., Kwon, M. and Spacone, E. (2005), "Analytical model of concrete-filled fiber-reinforced polymer tubes based on multiaxial constitutive laws", *J. Struct. Eng.*, **131**(9), 1426-1433.
- Cole, B. and Fam, A. (2006), "Flexural load testing of concrete-filled FRP tubes with longitudinal steel and FRP rebar", *J. Compos. Construct.*, **10**(2), 161-171.
- Davol, A., Burgueno, R. and Seible, F. (2001), "Flexural behavior of circular concrete filled FRP shell", *J. Struct. Eng.*, **127**(7), 810-817.
- Fam, A. and Rizkalla, S. (2002), "Flexural behavior of concrete-filled fiber-reinforced polymer circular tubes", *J. Compos. Construct.*, **6**(2), 123-132.
- Fujikake, K., Mindess, S. and Xu, H. (2004), "Analytical model for concrete confined with fibre reinforced polymer composite", *J. Compos. Construct.*, **8**(4), 341-351.
- Helmi, K., Fam, A. and Mufti, A. (2005), "Field installation, splicing, and flexural testing of hybrid FRP/concrete piles", *ACI Special Publication*, Vol. SP-230-62, 1103-1120.
- Hoult, N.A. and Lees, J.M. (2009), "Modeling of an unbonded CFRP strap shear retrofitting system for reinforced concrete beams", *J. Compos. Construct.*, **13**(4), 292-301.
- Hu, Y.M., Yu, T. and Teng, J.G. (2011), "FRP-confined circular concrete-filled thin steel tubes under axial compression", *J. Compos. Construct.*, **15**(5), 850-860.
- Lam, L. and Teng, J.G. (2004), "Ultimate condition of fibre reinforced polymer-confined concrete", *J. Compos. Construct.*, **8**(6), 539-548.
- Liu, L. and Lu, Y.Y. (2010), "Axial bearing capacity of short FRP confined concrete-filled steel tubular columns", *J. Wuhan Univ. Technol. (Materials Science)*, **25**(3), 454-458.
- Lu, G.C. (2005), "Study on behavior of concrete-filled FRP tubes under axial compression", Ph.D. Dissertation; Tsinghua University, Beijing, China. [In Chinese]
- Manjunatha, C.M., Taylor, A.C., Kinloch, A.J. and Sprenger, S. (2010), "The tensile fatigue behavior of a GFRP composite with rubber particle modified epoxy matrix", *J. Reinf. Plast. Compos.*, **29**(14), 2170-2183.
- Matthys, H., Toutanji, K. and Taerwe, L. (2005), "Axial load behaviour of large-scale columns confined with fibre-reinforced polymer composites", *ACI Struct. J.*, **102**(2), 258-267.
- Mehrdad, S.M. and Mohammad, H.R. (2009), "Experimental and analytical studies on one-way concrete slabs reinforced with GFRP molded gratings", *Steel Compos. Struct., Int. J.*, **9**(6), 569-584.
- Mirmiran, A., Shahawy, M. and Sammaan, M. (1999), "Strength and ductility of hybrid FRP-concrete beam-columns", *J. Struct. Eng.*, **125**(10), 1085-1093.
- Moran, D.A. and Pantelides, C.P. (2002), "Stress-strain model for fibre-reinforced polymer-confined concrete", *J. Compos. Construct.*, **6**(4), 233-240.
- Panda, K.C., Bhattacharyya, S.K. and Barai, S.V. (2012), "Shear behaviour of RC T-beams strengthened with U-wrapped GFRP sheet", *Steel Compos. Struct., Int. J.*, **12**(2), 149-166.
- Qin, G.P. (2009), "Mechanical behaviors study on GFRP tube filled with reinforced concrete members", Ph.D. Dissertation; Northeastern University, Shenyang, China. [In Chinese]
- Saadatmanesh, H. and Ehsani, M.R. (1994), "Strength and ductility of concrete external reinforced with fiber composite straps", *ACT Struct. J.*, **91**(4), 434-447.
- Saenz, N. and Pantelides, C.P. (2007), "Strain-based confinement model for FRP-confined concrete", *J. Struct. Eng.*, **133**(6), 825-833.
- Salim, H.A., Barker, M. and Davalos, J.F. (2006), "Approximate series solution for analysis of FRP composite highway bridges", *J. Compos. Construct.*, **10**(4), 357-366.
- Shao, Y. and Mirmiran, A. (2005), "Experimental Investigation of Cycled Behavior of Concrete Filled

- Fiber Reinforced Polymer Tubes”, *J. Compos. Construct.*, **9**(3), 263-273.
- Wang, B.L. and Wang, Q.X. (2009), “Research status of FRP tube filled with concrete composite structure”, *Ind. Construct. (supplement)*, **39**(437), 262-265. [In Chinese]
- Wang, Y.F., Ma, Y.S. and Wu, H.L. (2011), “Reinforced high-strength concrete square columns confined by aramid FRP jackets. part I: Experimental study”, *Steel Compos. Struct., Int. J.*, **11**(6), 455-468.
- Xiao, Y. and Wu, H. (2003), “Retrofit of reinforced concrete columns using partially stiffened steel jackets”, *J. Struct. Eng.*, **129**(6), 725-732.
- Xiong, W., Cai, C.S., Xiao, R.C. and Zhang, Y. (2012), “Design strategy of hybrid stay cable system using CFRP and steel materials”, *Steel Compos. Struct., Int. J.*, **13**(1), 47-70.
- Yu, T., Wong, Y.L., Teng, J.G., Dong, S.L. and Lam, E.S.S. (2006), “Flexural behavior of hybrid FRP-concrete- steel double skin tubular members”, *J. Compos. Construct.*, **10**(5), 443-452.
- Zhu, Z.Y., Ahmad, I. and Mirmiran, A. (2006), “Splicing of precast concrete-filled FRP tubes”, *J. Compos. Construct.*, **10**(4), 345-356.